HHS Public Access

Author manuscript

Nat Cell Biol. Author manuscript; available in PMC 2011 November 01.

Published in final edited form as:

Nat Cell Biol. 2011 May ; 13(5): 559–567. doi:10.1038/ncb2221.

ARFGAP1 promotes endocytosis regulated by AP-2

Ming Bai[1,10], **Helge Gad**[2,3,10], **Gabriele Turacchio**[2,4,10], **Emanuele Cocucci**[5], **Jia-Shu Yang**[1], **Jian Li**[1], **Galina V. Beznoussenko**[2], **Zhongzhen Nie**[6], **Rubai Luo**[7], **Lianwu Fu**[8], **James F. Collawn**[8], **Tomas Kirchhausen**[5], **Alberto Luini**[2,9], and **Victor W. Hsu**[1]

[1]Division of Rheumatology, Immunology and Allergy, Brigham and Women's Hospital, and Department of Medicine, Harvard Medical School, Boston, MA 02115 USA

[2]Department of Cell Biology and Oncology, Consorzio Mario Negri Sud, 66030 Santa Maria Imbaro (Chieti), Italy

[3]Department of Genetics, Microbiology and Toxicology, Stockholm University, 10691 Stockholm, Sweden

[4]Institute of Protein Biochemistry, National Research Council, Via Pietro Castellino 111, 80131 Naples, Italy

[5]Department of Cell Biology, Harvard Medical School, and Immune Disease Institute, Boston, MA 02115 USA

[6]Department of Urology, University of Florida College of Medicine Gainesville, FL 32610 USA

[7]Laboratory of Cellular and Molecular Biology, National Cancer Institute, Bethesda, MD 20892 USA

[8]Department of Cell Biology, University of Alabama at Birmingham, Birmingham, AL 35294 USA

[9]Telethon Institute of Genetics and Medicine, Via Pietro Castellino 111, 80131 Napoli, Italy

Abstract

Two of the best characterized coat proteins are Coat Protein (COP) I and clathrin associated with Adaptor Protein 2 (AP-2), for which no common component has been identified. A GTPase-activating protein (GAP) for ADP-Ribosylation Factor 1 (ARF1), ARFGAP1, is known to act as a component of the COPI complex. Here, we find that distinct regions of ARFGAP1 interact with AP-2 and coatomer (components of the COPI complex). Selectively disrupting the interaction of ARFGAP1 with either of these two coats leads to selective inhibition in the corresponding transport pathway. Elucidating how ARFGAP1 acts in endocytosis regulated by AP-2, we find mechanistic parallels to its elucidated roles in COPI transport, as both its GAP activity and its coat function contribute to promoting AP-2 transport.

Correspondence should be addressed to: VWH (vhsu@rics.bwh.harvard.edu).

[10]Equal contributions

AUTHOR CONTRIBUTIONS

MB, HG, GT, EC, JY, JL, GVB, ZN, and LF performed experiments and data analyses. VWH, AL, TK, and JC supervised the work. VWH, AL, HG, and MB wrote the manuscript.

Keywords

ARFGAP1; AP-2; clathrin; COPI; endocytosis

Coat proteins initiate vesicular transport by coupling vesicle formation with cargo sorting 1, 2. Currently, COPI, COPII, and the clathrin AP-2 complex are considered the best characterized coats 3–6. Coatomer was initially identified as components of the COPI complex 7. Sec13p, Sec23p, Sec24p, and Sec31p are considered the core components of the COPII complex 8. The clathrin triskelion combines with a hetero-tetrameric complex, known as the AP-2 adaptor, in forming a core complex 9, 10. Over the years, multiple auxiliary components have been identified for these major coats 11–15. However, despite their intense investigation, these complexes have not been observed to share a common component.

The ARF family of small GTPases regulates the recruitment of coat proteins to compartmental membrane 16. These small GTPases are regulated, in turn, by guanine nucleotide exchange factors (GEFs) that catalyze ARF activation 17, and GAPs that catalyze ARF deactivation 18. Besides this regulatory role, the best characterized ARF GAPs have also been shown to act as ARF effectors by being coat components. This role was first demonstrated for Sec23p, which acts both as the GAP for the small GTPase Sar1p and as a component of the COPII complex 8. ARFGAP1, a GAP for ARF1, has subsequently been shown to act similarly for the COPI complex 19, 20. We now show that ARFGAP1 also acts in endocytosis regulated by AP-2, with functional characterization suggesting that this unexpected role has mechanistic parallels to its elucidated functions in COPI transport.

RESULTS

ARFGAP1 acts directly in AP-2-dependent endocytosis of TfR

To gain new insight into how ARFGAP1 acts, we have been searching for interacting partners. In one approach, we incubated cytosol with beads that contained a glutathione-s-transferase (GST) fusion of ARFGAP1 (Fig 1a). Interacting proteins were then identified by mass spectrometry. Unexpectedly, we identified components of the clathrin AP-2 complex (Table S1). Thus, we initially further interrogated these suggested interactions by a co-precipitation approach, which also showed that ARFGAP1 interacted with components of the clathrin AP-2 complex (Fig 1b).

An interaction between ARFGAP1 and AP-2 had been detected previously 21, 22. Notably however, the functional significance of this interaction had not been explored. Thus, we next assessed whether key examples of clathrin-dependent endocytosis would be affected upon perturbing ARFGAP1. We depleted endogenous ARFGAP1 using small-interfering ribonucleic acid (siRNA) (Fig S1a), and found that transferrin (Tf) uptake was inhibited (Fig 1c), but not the uptake of epidermal growth factor (EGF) (Fig 1d) or low-density lipoprotein (LDL) (Fig 1e). This pattern of selective inhibition was similar to that seen previously upon the depletion of AP-2 23.

We further noted that another previous study had concluded that siRNA against ARFGAP1 did not affect Tf uptake 24. However, scrutiny of this previous study suggested a reconciling explanation. Technically, we bound Tf to the cell surface at 4°C followed by washing to release non-specific interactions. Cells were then warmed to 37°C to restore transport. Importantly, we also quantified the level of internalized Tf. In contrast, the previous contradictory study simply incubated cells with Tf continuously at 37°C, and then assessed Tf uptake qualitatively, by visual inspection 24. When we performed the Tf uptake by continuous incubation at 37°C, we could still detect inhibition in Tf uptake induced by siRNA against ARFGAP1, by quantifying the level of internalized Tf (Fig S1b). We also sought further confirmation using short-hairpin RNA (shRNA) that targeted a different sequence in ARFGAP1 (Fig S1c). Inhibition of Tf uptake was again observed (Fig S1d), and was further characterized by kinetic analysis (Fig S1e).

We next considered the possibility that the inhibition of Tf uptake upon the depletion of ARFGAP1 could be an indirect effect of having perturbed COPI transport that acts in the secretory pathway. To address this issue, we initially explored whether ARFGAP1 interacted differently with AP-2 versus coatomer. Generating different truncation mutants of ARFGAP1 as GST fusion proteins followed by incubation with cytosol, we found that coatomer bound to the extreme carboxy terminal region of ARFGAP1 (residues 401–415) (Fig 2a and Fig S2a). In contrast, AP-2 and clathrin interacted with a more proximal region of ARFGAP1 (residues 301–400) (Fig 2b). Within this region of ARFGAP1, we noted multiple tryptophan-based (WXXF/W) motifs (Fig S2b), which had been shown previously to mediate the binding of auxiliary proteins to AP-2 25, 26. Thus, we next examined the effect of mutating residues within these motifs in ARFGAP1.

One set of mutations involved substitutions at the second position of each motif (E330N/D364A/E383N, referred as EDE), which reduced the binding of ARFGAP1 to clathrin, but not to AP-2 (Fig 2c). Another set of mutations involved substitutions at the fourth position in each motif (F332A/W366A/W385A, referred as FWW), which reduced the binding of ARFGAP1 to both AP-2 and clathrin (Fig 2d). Notably, the binding of ARFGAP1 to coatomer was unaffected by either set of triple point mutations (Figs 2c and 2d). Thus, these results revealed distinct requirements for the binding of ARFGAP1 to AP-2 and clathrin versus coatomer (summarized in Fig 2e).

We next determined whether ARFGAP1 could interact directly with AP-2 and clathrin by using purified components. This approach revealed that ARFGAP1 interacted directly with AP-2 (Fig 3a), but not with clathrin (Fig 3b). Moreover, sequential incubations revealed that ARFGAP1 could interact with clathrin when AP-2 was first incubated with ARFGAP1 (Fig 3c). We also found that the FWW mutation in ARFGAP1 reduced its direct interaction with AP-2, while the EDE mutation had a milder effect (Fig 3a). Moreover, the EDE mutation in ARFGAP1 was observed to reduce the ability of AP-2 to link ARFGAP1 to clathrin, as assessed by sequential incubations of AP-2 followed by clathrin (Fig 3c). Thus, these results revealed that ARFGAP1 could interact directly with the AP-2 adaptor and only indirectly with the clathrin triskelion.

We next took advantage of these binding results to assess functionally whether ARFGAP1 acted in AP-2 transport independent of its role in COPI transport. Cells were depleted of ARFGAP1 to inhibit Tf uptake, and then the different mutant forms of the ARFGAP1 were assessed for their ability to rescue this defect. Technically, we performed all rescues by transfecting rat form of ARFGAP1, which was resistant to the targeting sequences used to deplete endogenous ARFGAP1 in primate cells. The two mutant forms of ARFGAP1 (FWW and EDE), which were found in the binding studies to have reduced ability to form a complex with AP-2 and clathrin, could not rescue defective Tf uptake (Fig 3d). In contrast, the wild-type and another mutant form of ARFGAP1 (a truncation form that spanned residues 1–400, which could not bind coatomer) rescued this defect (Fig 3d).

We also assessed whether the different mutations in ARFGAP1 affected retrograde COPI transport. A chimeric COPI cargo protein, known as VSVG-ts045-KDELR, had been generated to track this transport in vivo 27. At the non-permissive temperature, the misfolding of VSVG-ts045 prevents the chimera from exiting from the ER. Thus, because the KDELR cycles between the ER and the Golgi, inhibition of its anterograde transport allows the unambiguous tracking of its retrograde transport, which is COPI-dependent 28, 29. We found that the ARFGAP1 mutant that could not interact with coatomer (1–400) also could not rescue defective retrograde COPI transport induced by the depletion of endogenous ARFGAP1 (Fig 3e). In contrast, the wild-type and the two mutants that were defective in forming a complex with AP-2 and clathrin rescued this defect (Fig 3e). Thus, the rescue results revealed that ARFGAP1 acted in AP-2 transport independent of its role in COPI transport.

Surveying transport pathways that require ARFGAP1

The surface level of TfR is predicted to represent the balance between its rates of endocytosis and recycling. We found that this level was not appreciably altered by the depletion of ARFGAP1 (Fig 4a), which predicted that TfR recycling would also be affected by the perturbation. We confirmed this prediction by examining TfR recycling directly (Fig 4b). To determine whether this inhibition was an indirect effect of having inhibited TfR endocytosis, we again took advantage of ARFGAP1 mutants that were defective in binding to the AP-2 complex. These mutants were found to rescue the defective TfR recycling that had been induced by the depletion of endogenous ARFGAP1 (Fig 4c). Thus, we concluded that ARFGAP1 acted distinctly in TfR endocytosis versus recycling. In light of this finding, we next conducted a broader survey to determine whether ARFGAP1 could be acting in additional transport pathways.

Besides recycling to the plasma membrane (PM), endocytic cargoes are transported toward two other general destinations, the lysosomes or the Golgi. To survey endocytic transport to lysosomes, we tracked dextran, a fluid-phase marker, which also allowed us to examine pinocytosis (a type of non-clathrin endocytosis 30). We found that the internalization of dextran from the PM to early endosomes (EE) (Fig S3a), followed by its subsequent transport to lysosomes (Fig S3b), were not appreciably altered. To survey endocytic transport to the Golgi, we tracked the B subunit of cholera toxin (CTB), which also allowed us to examine yet another type of non-clathrin endocytosis (raft-dependent internalization)

30. We found that the internalization of CTB from the PM to EE (Fig S3c), followed by subsequent transport to the trans-Golgi network (TGN) (Fig S3d), were also unaffected. Thus, ARFGAP1 did not have widespread roles in endocytic pathways.

We next surveyed the secretory pathway by tracking a well characterized anterograde cargo, a temperature-sensitive form (ts-045) of the vesicular stomatitis virus G protein (VSVG) 31, 32. In cells depleted of ARFGAP1, we found that transport of this cargo from the ER to the TGN was slowed (Fig 4d). However, transport from the ER to the cis-side of the Golgi was unaffected (Fig 4e). Moreover, transport from the TGN to the PM was unaffected (Fig 4f). Taken together, these results suggested that only the intra-Golgi segment of the secretory pathway was delayed by the depletion of ARFGAP1, as would be predicted by its role in COPI transport. We also found that the depletion of ARFGAP1 had minimal effects on Golgi structure, as assessed at the level of both light (Fig S4a) and electron (Fig S4b) microscopy. Notably, similar findings had been observed by perturbing other critical components of COPI vesicle formation, such as BARS 28 and PLD2 29. In contrast, perturbation of coatomer 33 or ARF1 34 was observed previously to disrupt Golgi structure. Thus, we also concluded that ARF1 and coatomer would have additional roles, besides in COPI vesicular transport, in explaining why they are critical for Golgi structure.

ARFGAP1 promotes cargo sorting by AP-2

We next sought further insight into how ARFGAP1 could be acting in AP-2 transport, by initially determining its localization with respect to clathrin coated pits. Using the conventional approach of confocal microscopy, we found that the Golgi pool of ARFGAP1 emitted a sufficiently strong fluorescence to hamper the ability in detecting the peripheral pool of ARFGAP1. Thus, we next pursued total internal reflection fluorescence microscopy (TIR-FM) with live-imaging. We first confirmed that ARFGAP1 was still functional when coupled to the green fluorescent protein (GFP), as the fusion protein could still rescue the inhibition of Tf uptake induced by the depletion of ARFGAP1 (Fig S5a). Performing TIR-FM subsequently, we detected ARFGAP1 in clathrin coated pits (Fig 5a). Dynamic imaging revealed that ARFGAP1 associated transiently with clathrin coated structures mainly at the later stage of their lifetime (Fig 5b).

Next, pursuing quantitative electron microscopy (EM), we found that the level of coated pits was reduced in cells depleted of endogenous ARFGAP1 (Fig 5c). Thus, as coated pits internalize a broad range of cargoes 13, a prediction was that ARFGAP1 would be important for the endocytosis of more cargoes than just that of TfR. Supporting this prediction, we found that the endocytosis of cystic fibrosis transmembrane conductance regulator (CFTR), which had been shown to require AP-2 35, was also inhibited by the depletion of ARFGAP1 (Fig 5d). We next examined whether the depletion of ARFGAP1 arrested a particular stage of coated pit formation. However, no particular stage was observed to accumulate (Fig 5e). In considering how ARFGAP1 could be functioning to explain the noted effects on the level of coated pits and their formation, we considered that clathrin vesicle formation had been elucidated in recent years to have two general outcomes, either productive or abortive 36. As cargoes had been shown recently to promote the productive fate 37, 38, we next explored whether ARFGAP1 promoted cargo binding by AP-2.

Studying TfR as the model cargo, we initially determined whether ARFGAP1 could be detected to form an in vivo complex with surface TfR and AP-2. To examine only endogenous proteins, we bound biotin-conjugated Tf to the cell surface, and then lysed cells, followed by incubation with streptavidin-bound beads. Surface TfR was found to be associated with AP-2 and ARFGAP1 (Fig 6a). We also transfected GFP-tagged ARFGAP1 and found that it associated similarly with surface TfR and AP (Fig 6b), which further validated the observation above that this tagged ARFGAP1 could be detected in coated pits. In contrast, two other ARFGAPs, ARFGAP2 and ARFGAP3, could not interact with surface TfR (Fig 6c). Moreover, consistent with our initial finding that the endocytosis of the LDL receptor (LDLR) was not affected by the depletion of ARFGAP1, we found that a surface form of this receptor (CD8-LDLR, which was used previously to study the endocytosis of LDLR 23) did not interact with ARFGAP1 (Fig 6d). We also noted that previous studies had observed variable effects on LDL uptake upon the depletion of AP-2, with no inhibition detected by the traditional method of uptake (which involved binding at 4°C followed by incubation at 37°C) 23, while inhibition was detected by an alternate method (which involved continuous uptake at 37°C) 39. In contrast, we found that the depletion of ARFGAP1 inhibited Tf uptake using either method (see Fig 1c and Fig S1b). Thus, these observations further reinforced the specificity by which ARFGAP1 acted in the endocytosis of TfR.

We next considered that cargo sorting involves coat components binding directly to sorting signals in cargo proteins 1, 13. Thus, we examined whether ARFGAP1 could interact directly with two internalization sorting signals that had been identified in the cytoplasmic domain of TfR. One signal had been shown to require a critical phenylalanine at position 13 of TfR, while the other required a critical “YTRF” motif (positions 20–23) 40, 41. We generated a series of truncation constructs that encompassed the cytoplasmic domain of TfR (summarized in Fig S5b), and found that ARFGAP1 bound to the portion of the TfR cytoplasmic region that contained both internalization sorting signals (Fig 7a). Subsequently, examining truncations of TfR that possessed either of these two sorting signals, we found that ARFGAP1 could bind to either signal (Fig 7b). In contrast, AP-2 could only bind to the sorting signal defined by the “YTRF” motif (Fig 7c).

We also examined how mutations at the two sorting signals of TfR affected its association with ARFGAP1 and AP-2 in vivo. TfR had been shown to form homodimers 42. Thus, a transfected mutant TfR could potentially pair with endogenous wild-type TfR and thereby masking an effect of a particular mutation. To overcome this potential hurdle, we took advantage of a mutant cell line that lacked endogenous TfR 41. When different forms of TfR were transfected into this cell line, we found that mutations in one sorting signal (containing the “YTRF” motif) abrogated the association of TfR with AP-2 and ARFGAP1 more strongly than mutations in the other sorting signal (Fig 7d). Notably, we also found that the depletion of ARFGAP1 reduced the association of AP-2 with TfR in vivo (Fig 7e). Thus, the binding results altogether suggested that ARFGAP1 acted in promoting cargo sorting by AP-2.

Elucidating the role of the GAP activity in TfR endocytosis

As ARFGAP1 also possessed a GAP activity, we next examined whether this activity had a role in AP-2 transport. A point mutation in ARFGAP1 had been shown previously to abrogate its GAP activity 43. Whereas wild-type ARFGAP1 could rescue the defective Tf uptake induced by the depletion of endogenous ARFGAP1, we found that the catalytic-dead mutant could not (Fig 8a and Fig S5c). This result not only revealed a role for the GAP activity in AP-2 transport, but also implicated an ARF in this process. Consistent with ARF6 having been suggested to act in clathrin-mediated endocytosis 44–46, we next found that the depletion of ARF6 inhibited Tf uptake (Fig 8b). We also noted that the GAP activity of ARFGAP1 had only been well documented to act on ARF1. Thus, we revisited the in vitro GAP assay, and found that ARF6 could also be a substrate (Fig S5d). Furthermore, as coatomer had been shown previously to stimulate the GAP activity of ARFGAP1 toward ARF1 47, we found that AP-2 could also stimulate the GAP activity of ARFGAP1 toward ARF6 (Fig 8c).

Next, to gain insight into how the GAP activity of ARFGAP1 could be acting in TfR endocytosis, we initially found that ARF6 could bind directly to the cytoplasmic domain of TfR in an activation-dependent manner (Fig 8d). Moreover, ARF6 synergized with ARFGAP1 in enhancing the binding of AP-2 to TfR (Fig 8e). Notably, the GAP activity of ARFGAP1 further enhanced this binding, which was suggested by the observation that ARF6 preloaded with GTP allowed better binding of TfR by AP-2 than ARF6 loaded with a non-hydrolyzable analog of GTP (GTPγS) (Fig 8e). As confirmation, we found that the activation-dependent binding of ARF6 to TfR was abrogated when ARFGAP1 was added to the incubation, while this effect was prevented when ARF6 was preloaded with GTPγS. (Fig 8f). We also sought in vivo confirmation for key aspects of these in vitro findings. First, we confirmed that ARF6 bound to TfR in an activation-dependent manner, as the activating (Q67L), but not the deactivating (T27N), point mutant of ARF6 associated with surface TfR (Fig 8g). Second, we confirmed that ARF6 deactivation was important for the binding of AP-2 to surface TfR in vivo, as the expression of ARF6-Q67L reduced this association (Fig 8h). Altogether, these results suggested that at least one mechanism by which the GAP activity of ARFGAP1 promoted TfR endocytosis involved the optimization of cargo binding by AP-2.

DISCUSSION

We have found that ARFGAP1 promotes AP-2-dependent endocytosis. Characterizing this role, we have uncovered mechanistic parallels to how ARFGAP1 has been found previously to act in COPI transport, which involves dual roles as both ARF effector and regulator 6. ARFGAP1 binds to the two known sorting signals in TfR to promote endocytosis. Moreover, ARFGAP1 is needed to link AP-2 to TfR. These observations suggest that ARFGAP1 behaves as an ARF effector by acting as an auxiliary coat component to promote cargo sorting by AP-2. We also find that ARFGAP1 acts as an ARF6 regulator in AP-2-transport, as activated ARF6 that binds to TfR must be deactivated by the GAP activity of ARFGAP1 in optimizing the binding of TfR by AP-2.

AP-2 is now appreciated to act in at least two distinct stages. An initial stage involves AP-2 engaging a critical lipid, phosphatidylinositol 4,5-bisphosphate (PIP2), on the plasma membrane. A later stage involves AP-2 subsequently undergoing major conformational changes to open its binding sites for cargoes 48, 49. ARF6 has been shown previously to promote PIP2 production 44, 50. As such, it is predicted to act in the early stage of AP-2 action. However, our elucidation of how the GAP activity of ARFGAP1 promotes TfR endocytosis suggests an additional role for ARF6. This role is predicted to occur in the later stage of AP-2 action, which involves a complete GTPase cycle of ARF6 that optimizes cargo binding by AP-2. We further note that ARF1 deactivation has been shown previously to promote COPI cargo sorting 51, but the underlying mechanism has been unclear. Thus, as ARFGAP1 acts mechanistically similar in both AP-2 and COPI transport, our current elucidation of how its GAP activity promotes AP-2 cargo sorting likely represents new insight into how it acts in COPI cargo sorting.

METHODS

Proteins and antibodies

GST fusion and 6x-his-tagged recombinant proteins were purified as previously described 19. AP-2 and clathrin were purified as previously described 52. Alexa 546-conjugated Tf, Alexa 555-EGF, and Dil-LDL, and Alexa555-conjugated forms of dextran and CTB were obtained (Invitrogen).

The following antibodies were used, with dilution and source as indicated. Antibodies against the following proteins have been described previously 28, 53: ARF6 (1:200), ARFGAP1 (1:1000), BARS (1:2000), β2-adaptin (AP.6, 1:5000), β-COP (M3A5, 1:100, or culture supernatant, 1:10), CHC (TD.1, 1:500, or culture supernatant, 1:30), giantin (1:5000), Lamp1 (1:500), Myc epitope (9E10, 1:1000), TfR (5E9, 1:500, or H68.4, 1:1000), and VSVG (BW8G65, culture supernatant 1:10). Antibodies against other proteins were obtained: CD8 (1:400, Santa Cruz), EEA1 (1:200, BD Bioscience), HA epitope (HA.11, 1:1500, Covance), and TGN46 (1:1000, AbD Serotec).

Mass spectrometry

Cytosol was purified from rat brains by initially homogenizing in buffer B (25 mM Tris pH 8, 500 mM KCl, 250 mM sucrose, 2 mM EGTA, 1 mM DTT, plus protease inhibitors) at 4°C, followed by centrifugation at 5,000x g for 30 minutes and then 150,000x g for 90 minutes. The resulting supernatant was dialysed against buffer C (25 mM Tris pH 8, 50 mM KCl, 1 mM DTT), followed by centrifation at 150,000x g for 90 minutes at 4°C, and then stored at −80°C. GST-ARFGAP1 was crosslinked to glutathione sepharose by washing with sodium borate, incubation with DMP for 30 min followed by two washes with ethanol amine pH 8.2 and two washes with 0.1 M glycine pH 2.5. Beads were then incubated with or without 10 mg rat brain cytosol for 4 hours followed by extensive washing. Samples were separated by SDS-PAGE and then stained with silver chloride. Specific bands were excised for analysis by mass spectrometry (MSF facility, University of California, San Francisco, USA).

Plasmids, mutagenesis, and RNA interference

Constructs encoding for mutant forms of rat ARFGAP1 fused to GST were generated by PCR, digested with EcoRI (for forward primers) or XhoI (for reverse primers), and inserted into the pGEX-6P1 vector (Amersham) using the Rapid ligation kit (Promega). Site-directed mutagenesis was performed with the QuikChange site-directed mutagenesis kit (Stratagene), and then verified by sequencing. Multi-site mutagenesis PCR was performed by addition of Taq ligase (New England Biolabs), 0.5x ligase buffer and mutant primers annealing only to the lower DNA strand. All constructs were verified by DNA sequencing (MWG Biotech). Other constructs have been previously described, including ARFGAP1-myc 20, mutant forms of the TfR cytoplasmic domain as GST fusion constructs 54, VSVG-KDELR-YFP 29, and clathrin light chain tagged with mCherry36. Additional constructs were obtained: GFP-ARFGAP1 (gift from D. Cassel, Technion, Israel), and VSVG-ts045-GFP and VSVG-ts045-KDELR (J. Lippincott-Schwartz, NIH, USA).

Nucleotides 206 to 224 of human ARFGAP1 were targeted for siRNA (ACAUUGAGCUUGAGAAGAU; Dharmacon), while nucleotides 297 to 318 of human ARFGAP1 were targeted for shRNA (ACAGGAGAAGUACAACAGCAGA; Thermal Scientific). A lentivirus expression system (Thermal Scientific) was used for the stable expression of shRNA in BSC-1 cells.

Transfections

FuGene 6 (Roche) was used to transfect DNA plasmids, and Oligofectamine (Invitrogen) or Lipofectamine RNAiMax (Invitrogen) was used to transfect siRNA oligonucleotides, all according to manufacturers' guidelines.

Pulldown assays

GST fusion proteins on glutathione beads were incubated with soluble proteins (4 nM – 10 nM) at 4°C for 1 hour in 0.5 ml of a buffer that contained 50mM HEPES (pH 7.3), 300mM NaCl, 90mM KCl, 1mM EDTA and 0.5% NP-40. After this incubation, beads were pelleted by centrifugation (1000x g for 1 minute at 4°C) followed by two washes with the incubation buffer, and then analyzed by SDS-PAGE followed by western blotting. Coomassie blue staining was performed to detect the level of GST fusion proteins on beads. In experiments that assessed how GAP activity modulates the binding of AP-2 to TfR, a modified buffer was used (to allow more efficient GAP activity), which contained 50mM HEPES (pH 7.3), 300mM NaCl, 90mM KCl, 1mM $MgCl_2$ and 0.5% NP-40.

In vivo assays

To detect proteins associated with surface TfR, intact cells were initially bound by biotin-labelled Tf at 4°C. Cells were then lysed followed by incubation with beads coated with streptavidin. Beads were then washed, loaded onto SDS-PAGE gel followed by immunoblotting.

The uptake of Tf, EGF, and LDL was performed using a fluorescence-based approach, as previously described 32. Tf uptake was also quantified by a biochemical approach. Briefly, biotin-conjugated Tf was bound to intact cells at 4°C, followed by washing with

DMEM/PBS to release non-specific binding. Cells were then warmed to 37°C to initiate endocytosis for times indicated. Afterwards, cells were washed with ice-cold DMEM/PBS to arrest transport, followed by washes with an acid-based buffer (0.5M NaCl and 0.5% acetic acid) to release biotin-Tf that remained bound to the cell surface. Cells were then lysed followed by SDS/PAGE analysis, and then detection with horseradish peroxidase (HRP)-conjugated streptavidin. The level of internalized biotin-Tf was normalized to those initially bound to the cell surface in calculating the fraction of TfR internalized.

TfR recycling was performed by first incubating biotin-conjugated Tf with cells at 37°C for 2 hours. Cells were then shifted to 4°C for washes with an acid-based buffer (0.5M NaCl and 0.5% acetic acid) to release biotin-Tf that remained bound to the cell surface. To measure recycling, cells were then warmed to 37°C to restore transport, followed by another acid-wash. Cells were then lysed followed by SDS/PAGE analysis, and then detection with HRP-conjugated streptavidin. For quantitation, the level of internal biotin-Tf was normalized to the level of biotin-Tf within cells at the start of recycling in order to calculate the fraction of internal Tf remaining at different time points.

To assess transport from the plasma membrane to the early endosome, and subsequently to the lysosome, fluorescence-conjugated dextran was incubated with cells at 37°C for times indicated. Colocalization was then performed with markers of the early endosome (EEA1) and the lysosome (Lamp1). To assess transport from the plasma membrane to the early endosome, and subsequently to the TGN, fluorescence-conjugated CTB was bound to the cell surface at 4°C. Cells were then washed with PBS, followed by warming to 37°C for times indicated. Colocalization was then performed with markers of the early endosome (EEA1) and the TGN (TGN46). Confocal images were obtained using an inverted microscope (TE2000, Nikon) with C1 confocal system. Quantitation of colocalization was performed as previously described 53.

Other in vivo transport assays have been described, including anterograde transport of VSVG-ts045 55, the redistribution of VSVG-ts045-KDELR from the Golgi to the ER to assess retrograde COPI-dependent transport 29. Endocytosis of surface CTFR in polarized CFBE41o-cells has also been described previously 56. In particular, polarized monolayers were cultured to attain a resistance of ~400 ohm-cm^2, which typically occurred after 4 days.

In vitro GAP assay

This assay was performed essentially as previously described 57. Briefly, large unilamellar vesicles (LUVs) consisting of 40% phosphatidylcholine, 25% phosphatidylethanolamine, 15% phosphatidylserine, 10% phosphatidylinositol and 10% cholesterol (Avanti Polar Lipids, Inc., Alabaster, AL), were prepared by extrusion. Recombinant ARF1 or ARF6 was loaded with [α-^{32}P]GTP at 30°C for 30 min in the presence of LUVs with 500 μM lipid in the GTP loading buffer (25 mM HEPES, pH 7.4, 100 mM NaCl, 0.5 mM $MgCl_2$, 1 mM EDTA, 1 mM ATP and 1 mM DTT). GTP hydrolysis was initiated by adding recombinant ARFGAP1 at different concentrations, and either with or without AP-2 (175 nM), to [α-^{32}P]GTP loaded ARF6 (1 μM) in GAP assay buffer (25 mM HEPES, pH 7.4, 100 mM NaCl, 2 mM $MgCl_2$, 1 mM GTP, 1 mM DTT).

Electron microscopy

Cells grown on 35 mm glass bottom dishes (MatTek corporation) were fixed with 1% glutaraldehyde in 100 mM Hepes pH 7.4 overnight, washed several times with 100 mM Hepes pH 7.4, once with double-distilled water and post-fixed with 1% OsO_4, 1.5% $Na_4Fe(CN)_6$ in 0.1 M Cacodylate buffer pH 7.4 for 1 hour at room temperature. Samples were washed with double-distilled water, dehydrated with ethanol and embedded in Epon. Serial sections were counterstained with 1% lead citrate and then observed by EM. Quantitation of coated pits was performed on random images taken at 43,000 x magnification.

TIR-FM and live imaging

The Mariana™ system (Intelligent Imaging Innovations, Denver CO) based on a 200M inverted microscope and TIRF slider with manual angle and focus controls (Zeiss) was used. Images were acquired with an oil immersion Alpha Plan-Apo 100X objective (1.46 NA). A spherical aberration correction unit (Intelligent Imaging Innovations) was inserted into the emission path. Images were acquired with an electron multiplying charge coupled device (EMCCD) camera (QuantEM, Photometrics). Microscope operation and image acquisition were controlled using SlideBook software (V4.2.12, Intelligent Imaging Innovations). Time-lapse images were acquired sequentially for each wavelength using exposures of 30msec and at intervals of 3 seconds. The incidence angle of the excitation beam was adjusted so as to generate an evanescence field (with a penetration depth between 100–200 nm).

Statistical analysis

The Student’s t-test was performed to analyze statistical significance.

Supplementary Material

Refer to Web version on PubMed Central for supplementary material.

ACKNOWLEDGEMENT

We thank Beverly Wendland for critical comments. This work was funded by grants from the National Institutes of Health to VWH (GM058615 and GM073016), TK (GM075252 and U54 AI057159), and JFC (DK060065). AL was funded by the Telethon (Italy) and AIRC (Italy). HG was supported by a Marie Curie Fellowship. EC was supported by a GlaxoSmithKline fellowship.

REFERENCES

1. Bonifacino JS, Glick BS. The mechanisms of vesicle budding and fusion. Cell. 2004; 116:153–166. [PubMed: 14744428]
2. Cai H, Reinisch K, Ferro-Novick S. Coats, tethers, Rabs, and SNAREs work together to mediate the intracellular destination of a transport vesicle. Dev Cell. 2007; 12:671–682. [PubMed: 17488620]
3. Lee MC, Miller EA, Goldberg J, Orci L, Schekman R. Bi-directional protein transport between the ER and Golgi. Annu Rev Cell Dev Biol. 2004; 20:87–123. [PubMed: 15473836]
4. McMahon HT, Mills IG. COP and clathrin-coated vesicle budding: different pathways, common approaches. Curr Opin Cell Biol. 2004; 16:379–391. [PubMed: 15261670]
5. Pucadyil TJ, Schmid SL. Conserved functions of membrane active GTPases in coated vesicle formation. Science. 2009; 325:1217–1220. [PubMed: 19729648]

6. Hsu VW, Lee SY, Yang JS. The evolving understanding of COPI vesicle formation. Nat Rev Mol Cell Biol. 2009; 10:360–364. [PubMed: 19293819]
7. Waters MG, Serafini T, Rothman JE. 'Coatomer': a cytosolic protein complex containing subunits of non-clathrin-coated Golgi transport vesicles. Nature. 1991; 349:248–251. [PubMed: 1898986]
8. Barlowe C, et al. COPII: a membrane coat formed by Sec proteins that drive vesicle budding from the endoplasmic reticulum. Cell. 1994; 77:895–907. [PubMed: 8004676]
9. Pearse BMF. Coated vesicles from pig brain: purification and biochemical characterization. J. Mol. Biol. 1975; 97:93–98. [PubMed: 1177317]
10. Pearse BM, Robinson MS. Purification and properties of 100-kd proteins from coated vesicles and their reconstitution with clathrin. EMBO Journal. 1984; 3:1951–1957. [PubMed: 6149117]
11. Maldonado-Baez L, Wendland B. Endocytic adaptors: recruiters, coordinators and regulators. Trends Cell Biol. 2006; 16:505–513. [PubMed: 16935508]
12. Ungewickell EJ, Hinrichsen L. Endocytosis: clathrin-mediated membrane budding. Curr Opin Cell Biol. 2007; 19:417–425. [PubMed: 17631994]
13. Traub LM. Tickets to ride: selecting cargo for clathrin-regulated internalization. Nat Rev Mol Cell Biol. 2009; 10:583–596. [PubMed: 19696796]
14. Hsu VW, Yang JS. Mechanisms of COPI vesicle formation. FEBS Lett. 2009; 583:3758–3763. [PubMed: 19854177]
15. Miller EA, Barlowe C. Regulation of coat assembly--sorting things out at the ER. Curr Opin Cell Biol. 2010; 22:447–453. [PubMed: 20439155]
16. D'Souza-Schorey C, Chavrier P. ARF proteins: roles in membrane traffic and beyond. Nat Rev Mol Cell Biol. 2006; 7:347–358. [PubMed: 16633337]
17. Casanova JE. Regulation of Arf activation: the Sec7 family of guanine nucleotide exchange factors. Traffic. 2007; 8:1476–1485. [PubMed: 17850229]
18. Inoue H, Randazzo PA. Arf GAPs and Their Interacting Proteins. Traffic. 2007; 8:1465–1475. [PubMed: 17666108]
19. Yang JS, et al. ARFGAP1 promotes the formation of COPI vesicles, suggesting function as a component of the coat. J Cell Biol. 2002; 159:69–78. [PubMed: 12379802]
20. Lee SY, Yang JS, Hong W, Premont RT, Hsu VW. ARFGAP1 plays a central role in coupling COPI cargo sorting with vesicle formation. J Cell Biol. 2005; 168:281–290. [PubMed: 15657398]
21. Schmid EM, et al. Role of the AP2 beta-appendage hub in recruiting partners for clathrin-coated vesicle assembly. PLoS Biol. 2006; 4:e262. [PubMed: 16903783]
22. Rawet M, Levi-Tal S, Szafer-Glusman E, Parnis A, Cassel D. ArfGAP1 interacts with coat proteins through tryptophan-based motifs. Biochem Biophys Res Commun. 2010; 394:553–557. [PubMed: 20211604]
23. Motley A, Bright NA, Seaman MN, Robinson MS. Clathrin-mediated endocytosis in AP-2-depleted cells. J Cell Biol. 2003; 162:909–918. [PubMed: 12952941]
24. Saitoh A, Shin HW, Yamada A, Waguri S, Nakayama K. Three homologous ArfGAPs participate in coat protein I-mediated transport. J Biol Chem. 2009; 284:13948–13957. [PubMed: 19299515]
25. Mishra SK, et al. Dual engagement regulation of protein interactions with the AP-2 adaptor alpha appendage. J Biol Chem. 2004; 279:46191–46203. [PubMed: 15292237]
26. Praefcke GJ, et al. Evolving nature of the AP2 alpha-appendage hub during clathrin-coated vesicle endocytosis. Embo J. 2004; 23:4371–4383. [PubMed: 15496985]
27. Cole NB, Ellenberg J, Song J, DiEuliis D, Lippincott-Schwartz J. Retrograde transport of Golgi-localized proteins to the ER. J Cell Biol. 1998; 140:1–15. [PubMed: 9425149]
28. Yang JS, et al. A role for BARS at the fission step of COPI vesicle formation from Golgi membrane. EMBO J. 2005; 24:4133–4143. [PubMed: 16292346]
29. Yang JS, et al. A role for phosphatidic acid in COPI vesicle fission yields insights into Golgi maintenance. Nat Cell Biol. 2008; 10:1146–1153. [PubMed: 18776900]
30. Conner SD, Schmid SL. Regulated portals of entry into the cell. Nature. 2003; 422:37–44. [PubMed: 12621426]
31. Presley JF, et al. ER-to-Golgi transport visualized in living cells. Nature. 1997; 389:81–85. [PubMed: 9288971]

32. Bonazzi M, et al. CtBP3/BARS drives membrane fission in dynamin-independent transport pathways. Nat Cell Biol. 2005; 7:570–580. [PubMed: 15880102]
33. Guo Q, Vasile E, Krieger M. Disruptions in Golgi structure and membrane traffic in a conditional lethal mammalian cell mutant are corrected by epsilon-COP. J Cell Biol. 1994; 125:1213–1224. [PubMed: 8207054]
34. Dascher C, Balch WE. Dominant inhibitory mutants of ARF1 block endoplasmic reticulum to Golgi transport and trigger disassembly of the Golgi apparatus. J Biol Chem. 1994; 269:1437–1448. [PubMed: 8288610]
35. Weixel KM, Bradbury NA. Mu 2 binding directs the cystic fibrosis transmembrane conductance regulator to the clathrin-mediated endocytic pathway. J Biol Chem. 2001; 276:46251–46259. [PubMed: 11560923]
36. Ehrlich M, et al. Endocytosis by random initiation and stabilization of clathrin-coated pits. Cell. 2004; 118:591–605. [PubMed: 15339664]
37. Loerke D, et al. Cargo and dynamin regulate clathrin-coated pit maturation. PLoS Biol. 2009; 7:e57. [PubMed: 19296720]
38. Mettlen M, Loerke D, Yarar D, Danuser G, Schmid SL. Cargo- and adaptor-specific mechanisms regulate clathrin-mediated endocytosis. J Cell Biol. 2010; 188:919–933. [PubMed: 20231386]
39. Boucrot E, Saffarian S, Zhang R, Kirchhausen T. Roles of AP-2 in clathrin-mediated endocytosis. PloS one. 2010; 5:e10597. [PubMed: 20485680]
40. Collawn JF, et al. Transferrin receptor internalization sequence YXRF implicates a tight turn as the structural recognition motif for endocytosis. Cell. 1990; 63:1061–1072. [PubMed: 2257624]
41. McGraw TE, Pytowski B, Arzt J, Ferrone C. Mutagenesis of the human transferrin receptor: two cytoplasmic phenylalanines are required for efficient internalization and a second-site mutation is capable of reverting an internalization-defective phenotype. J Cell Biol. 1991; 112:853–861. [PubMed: 1900298]
42. Alvarez E, Girones N, Davis RJ. Intermolecular disulfide bonds are not required for the expression of the dimeric state and functional activity of the transferrin receptor. Embo J. 1989; 8:2231–2240. [PubMed: 2507316]
43. Szafer E, et al. Role of coatomer and phospholipids in GTPase-activating protein-dependent hydrolysis of GTP by ADP-ribosylation factor-1. J Biol Chem. 2000; 275:23615–23619. [PubMed: 10811810]
44. Krauss M, et al. ARF6 stimulates clathrin/AP-2 recruitment to synaptic membranes by activating phosphatidylinositol phosphate kinase type Igamma. J Cell Biol. 2003; 162:113–124. [PubMed: 12847086]
45. Palacios F, Schweitzer JK, Boshans RL, D'Souza-Schorey C. ARF6-GTP recruits Nm23-H1 to facilitate dynamin-mediated endocytosis during adherens junctions disassembly. Nat Cell Biol. 2002; 4:929–936. [PubMed: 12447393]
46. Paleotti O, et al. The small G-protein Arf6GTP recruits the AP-2 adaptor complex to membranes. J Biol Chem. 2005; 280:21661–21666. [PubMed: 15802264]
47. Goldberg J. Decoding of sorting signals by coatomer through a GTPase switch in the COPI coat complex. Cell. 2000; 100:671–679. [PubMed: 10761932]
48. Jackson LP, et al. A large-scale conformational change couples membrane recruitment to cargo binding in the AP2 clathrin adaptor complex. Cell. 2010; 141:1220–1229. [PubMed: 20603002]
49. Rapoport I, et al. Regulatory interactions in the recognition of endocytic sorting signals by AP-2 complexes. Embo J. 1997; 16:2240–2250. [PubMed: 9171339]
50. Honda A, et al. Phosphatidylinositol 4-phosphate 5-kinase alpha is a downstream effector of the small G protein ARF6 in membrane ruffle formation. Cell. 1999; 99:521–532. [PubMed: 10589680]
51. Lanoix J, et al. GTP hydrolysis by arf-1 mediates sorting and concentration of Golgi resident enzymes into functional COP I vesicles. Embo J. 1999; 18:4935–4948. [PubMed: 10487746]
52. Matsui W, Kirchhausen T. Stabilization of clathrin coats by the core of the clathrin-associated protein complex AP-2. Biochemistry. 1990; 29:10791–10798. [PubMed: 2125494]
53. Li J, et al. An ACAP1-Containing Clathrin Coat Complex for Endocytic Recycling. J Cell Biol. 2007; 178:453–464. [PubMed: 17664335]

54. Dai J, et al. ACAP1 Promotes Endocytic Recycling by Recognizing Recycling Sorting Signals. Dev Cell. 2004; 7:771–776. [PubMed: 15525538]

55. Trucco A, et al. Secretory traffic triggers the formation of tubular continuities across Golgi sub-compartments. Nat Cell Biol. 2004; 6:1071–1081. [PubMed: 15502824]

56. Peter K, et al. Ablation of internalization signals in the carboxyl-terminal tail of the cystic fibrosis transmembrane conductance regulator enhances cell surface expression. J Biol Chem. 2002; 277:49952–49957. [PubMed: 12376531]

57. Che MM, Nie Z, Randazzo PA. Assays and properties of the Arf GAPs AGAP1, ASAP1, and Arf GAP1. Methods Enzymol. 2005; 404:147–163. [PubMed: 16413266]

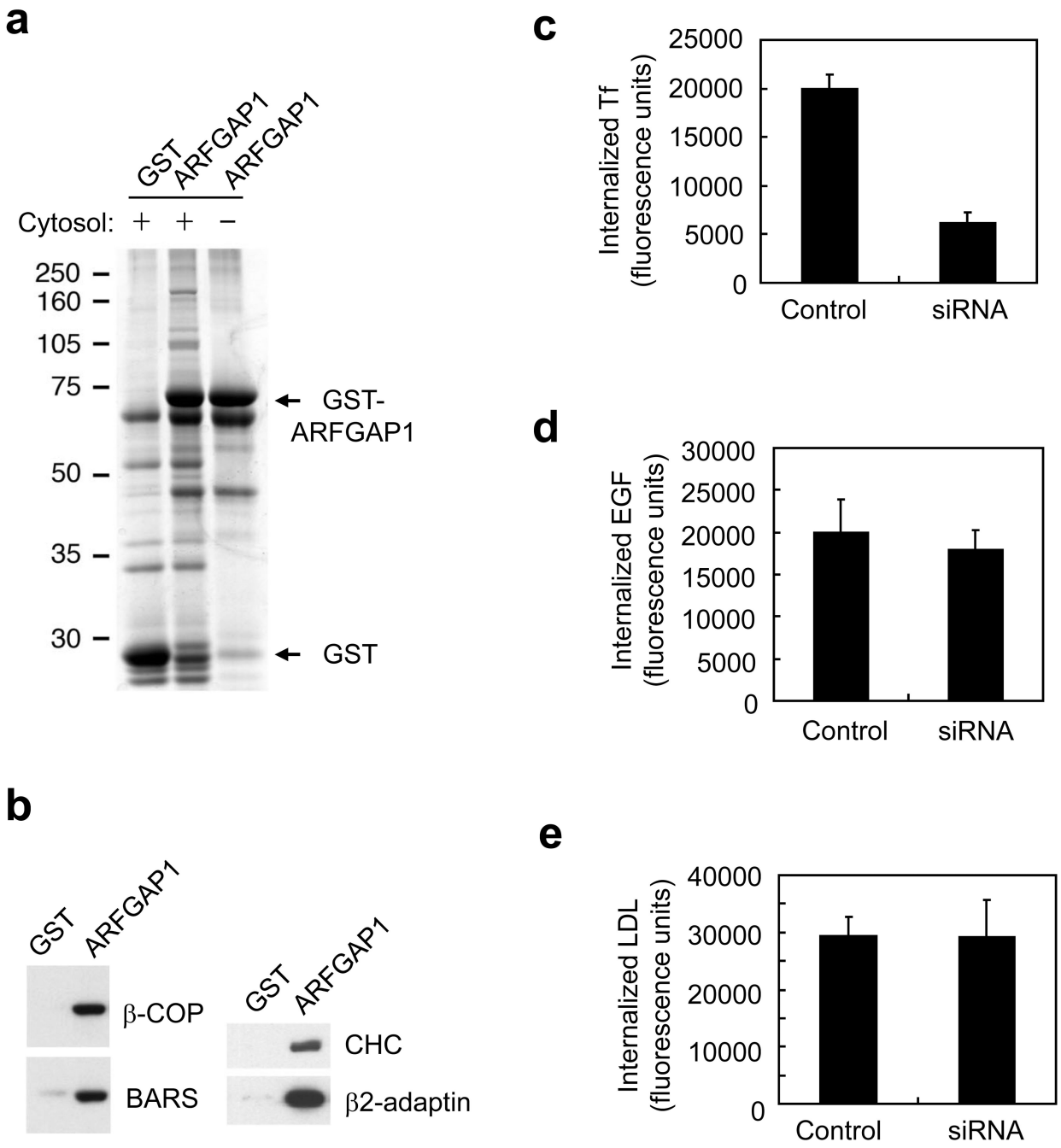

Figure 1. Interactions with ARFGAP1 and effects of its knockdown

a. Pull-down assay detects proteins interacting with ARFGAP1. ARFGAP1 as a GST fusion protein was bound to glutathione beads, incubated with cytosol, and then analyzed for associated proteins by Coomassie staining.

b. Pull-down assay detects ARFGAP1 interacting with coat components. ARFGAP1 as a GST fusion protein was bound to glutathione beads, incubated with cytosol, and then immunoblotted for proteins as indicated. ARFGAP1 interacts with components of AP-2, and also with previously known interacting proteins that are components of the COPI complex.

c. Tf uptake is reduced by siRNA against ARFGAP1. BSC-1 cells were bound with fluorescence-conjugated Tf, and then assessed for the level of internalized Tf at 10 minutes. The mean from three experiments with standard error is shown. Difference between the two conditions is significant ($p<0.05$).

d. EGF uptake is not markedly affected by siRNA against ARFGAP1. BSC-1 cells were with fluorescence-conjugated EGF, and then assessed for the level of internalized EGF at 10 minutes. The mean from three experiments with standard error is shown. Difference between the two conditions is insignificant ($p>0.05$).

e. LDL uptake is not markedly affected by siRNA against ARFGAP1. BSC-1 cells were bound with fluorescence-conjugated LDL, and then assessed for the level of internalized LDL at 10 minutes. The mean from three experiments with standard error is shown. Difference between the two conditions is insignificant ($p>0.05$).

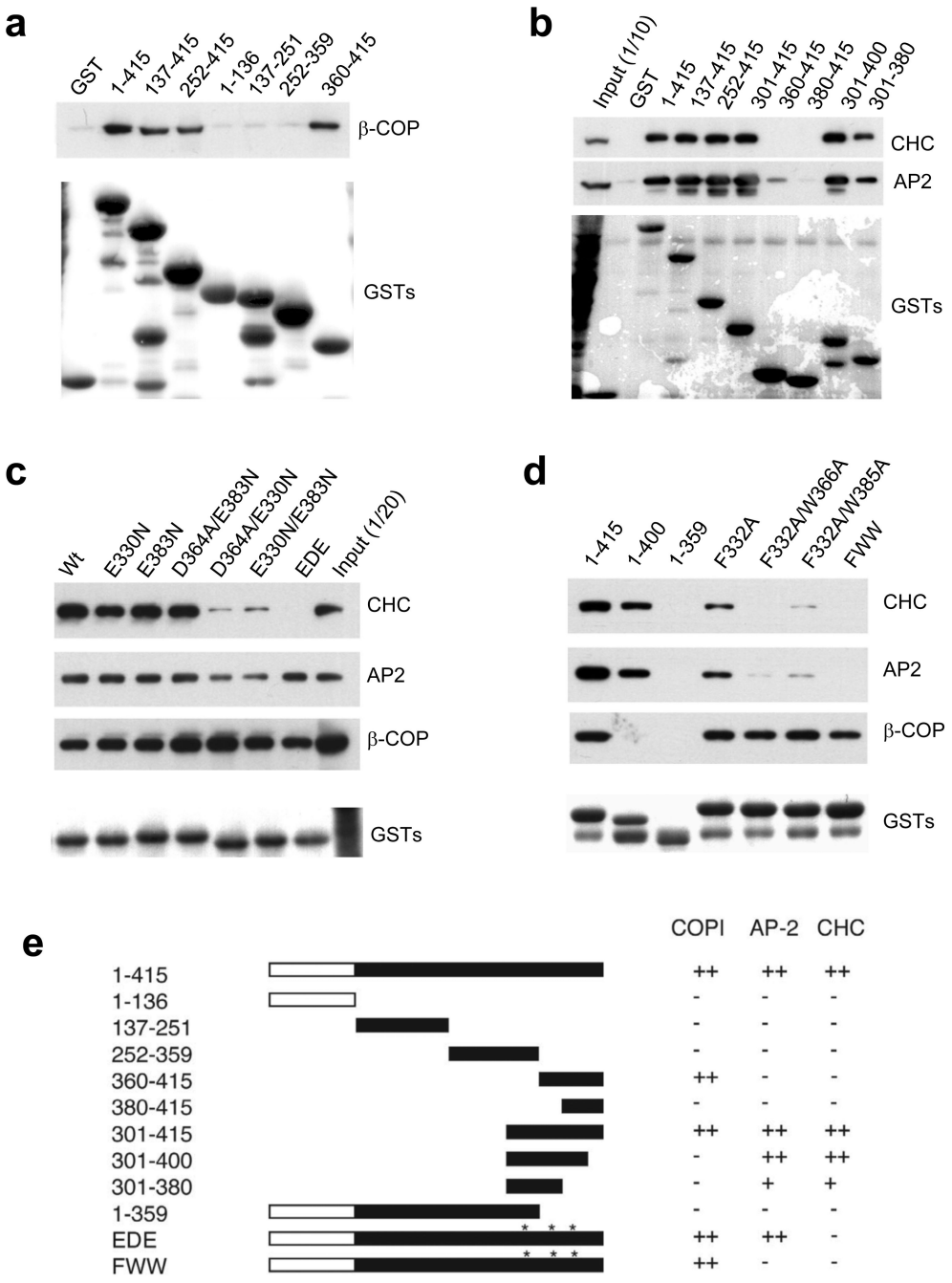

Figure 2. Distinct requirements for ARFGAP1 binding to coatomer versus AP-2 and clathrin

a. Interaction of different truncation mutants of ARFGAP1 with coatomer. The different forms of ARFGAP1 as GST fusion proteins were bound to beads, incubated with cytosol, and then immunoblotted for proteins as indicated. GST fusion proteins were detected by Coomassie staining.

b. Interaction of different truncation mutants of ARFGAP1 with AP-2 or clathrin. Pulldown experiments were performed as described above.

c. Interaction of different point mutants of ARFGAP1 with AP-2, clathrin, or coatomer. Pulldown experiments were performed as described above.
d. Interaction of additional mutants of ARFGAP1 with AP-2, clathrin, or coatomer. Pulldown experiments were performed as described above.
e. Interactions of ARFGAP1 with AP-2, clathrin and coatomer are summarized. The catalytic domain of ARFGAP1 is shown in white. Asterisks indicate W-box motifs.

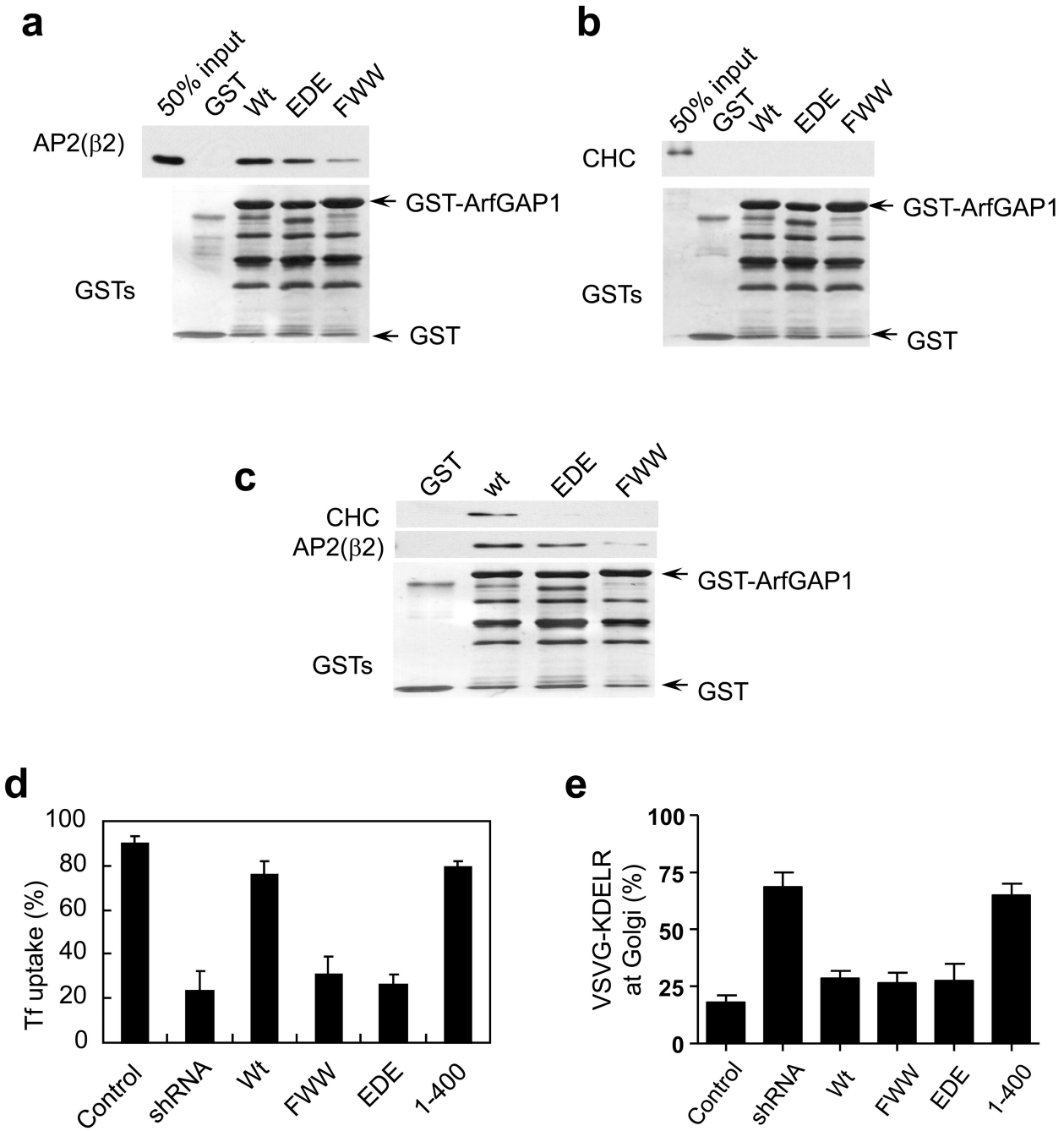

Figure 3. Disrupting interaction with either coatomer or AP-2 leads to selective disruption in transport pathways

a. Pulldown assays to assess direct binding of ARFGAP1 to AP-2. The different forms of ARFGAP1 as GST fusion proteins were bound to beads, incubated with purified AP-2 adaptors, and then immunoblotted for proteins as indicated. GST fusion proteins were detected by Coomassie staining.

b. Pulldown assays to assess direct binding of ARFGAP1 to clathrin. The different forms of ARFGAP1 as GST fusion proteins were bound to beads, incubated with purified clathrin

triskelia, and then immunoblotted for proteins as indicated. GST fusion proteins were detected by Coomassie staining.

c. Sequential incubations reveal that the AP-2 adaptor is needed to link ARFGAP1 to the clathrin triskelion. The different forms of ARFGAP1 as GST fusion proteins were bound to beads, and then incubated with purified AP-2 followed by incubation with purified clathrin. Beads were then analyzed by immunoblotted for proteins as indicated. GST fusion proteins were detected by Coomassie staining.

d. Rescue of defective Tf uptake induced by the depletion of ARFGAP1. BSC-1 cells that stably expressed shRNA against ARFGAP1 were transfected with different rat forms of ARFGAP1 as indicated. Uptake of biotin-Tf at 10 minutes was then quantified. The mean from three experiments with standard error is shown. Difference among conditions of shRNA, FWW and EDE are insignificant ($p>0.05$). Difference between this group and all other conditions are significant ($p<0.05$).

e. Rescue of defective COPI transport induced by the depletion of ARFGAP1. BSC-1 cells that stably expressed shRNA against ARFGAP1 were transfected with different rat forms of ARFGAP1 as indicated. The redistribution of VSVG-KDELR from the Golgi to the ER at 30 minutes was then quantified. The mean from three experiments with standard error is shown. Difference among conditions of Wt, FWW and EDE are insignificant ($p>0.05$). Difference between this group and conditions of shRNA and 1–400 are significant ($p<0.05$).

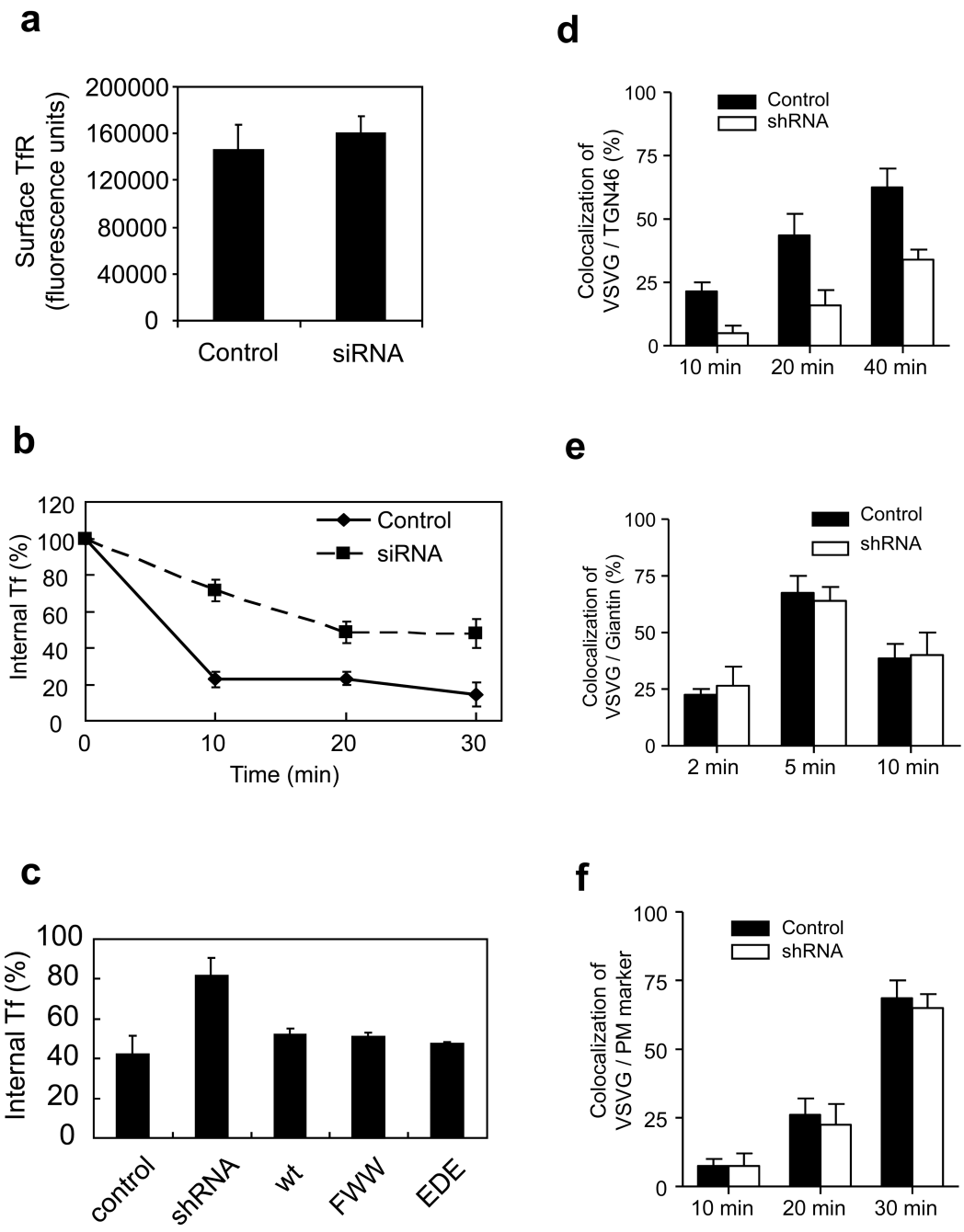

Figure 4. Surveying transport pathways affected by the depletion of ARFGAP1

a. Surface level of TfR is not affected by ARFGAP1 depletion. An antibody that recognizes the extracellular domain of TfR was bound to BSC-1 cells, followed by quantitation. The mean from three experiments with standard error is shown. Difference between the two conditions is insignificant ($p>0.05$).

b. TfR recycling is reduced by siRNA against ARFGAP1. BSC-1 cells were treated with siRNA against ARFGAP1, and then the level of internal biotin-Tf at time points as indicated

was quantified. The mean from three experiments with standard error is shown. Difference between the two conditions (except time = 0) is significant ($p<0.05$).

c. Rescue of defective TfR recycling induced by the depletion of ARFGAP1. BSC-1 cells that stably expressed shRNA against ARFGAP1 were transfected with different forms of rat ARFGAP1 as indicated. The level of internal biotin-Tf that remained was then quantified. The mean with standard error from three experiments is shown. Difference between shRNA and all other conditions is significant ($p<0.05$).

d. Depletion of ARFGAP1 inhibits transport from the ER to the TGN. VSVG-ts045 was transfected into BSC-1 cells, followed by quantitation of its colocalization with a TGN marker (TGN46). The mean from three experiments with standard error is shown. Difference at all time points is significant ($p<0.05$).

e. Depletion of ARFGAP1 does not affect transport from the ER to the cis-side of the Golgi. VSVG-ts045 was transfected into BSC-1 cells, followed by quantitation of its colocalization with a cis-Golgi marker (giantin). The mean from three experiments with standard error is shown. Difference at all time points is insignificant ($p>0.05$).

f. Depletion of ARFGAP1 does not affect transport from the TGN to the PM. VSVG-ts045 was transfected into BSC-1 cells, and then accumulated at the TGN. Cells were then shifted from 20°C to 32°C to allow transport to the plasma membrane (PM). Arrival of VSVG at the PM was detected through colocalization with fluorescence-conjugated CTB (which was bound to the cell surface). The mean from three experiments with standard error is shown. Difference at all time points is insignificant ($p>0.05$).

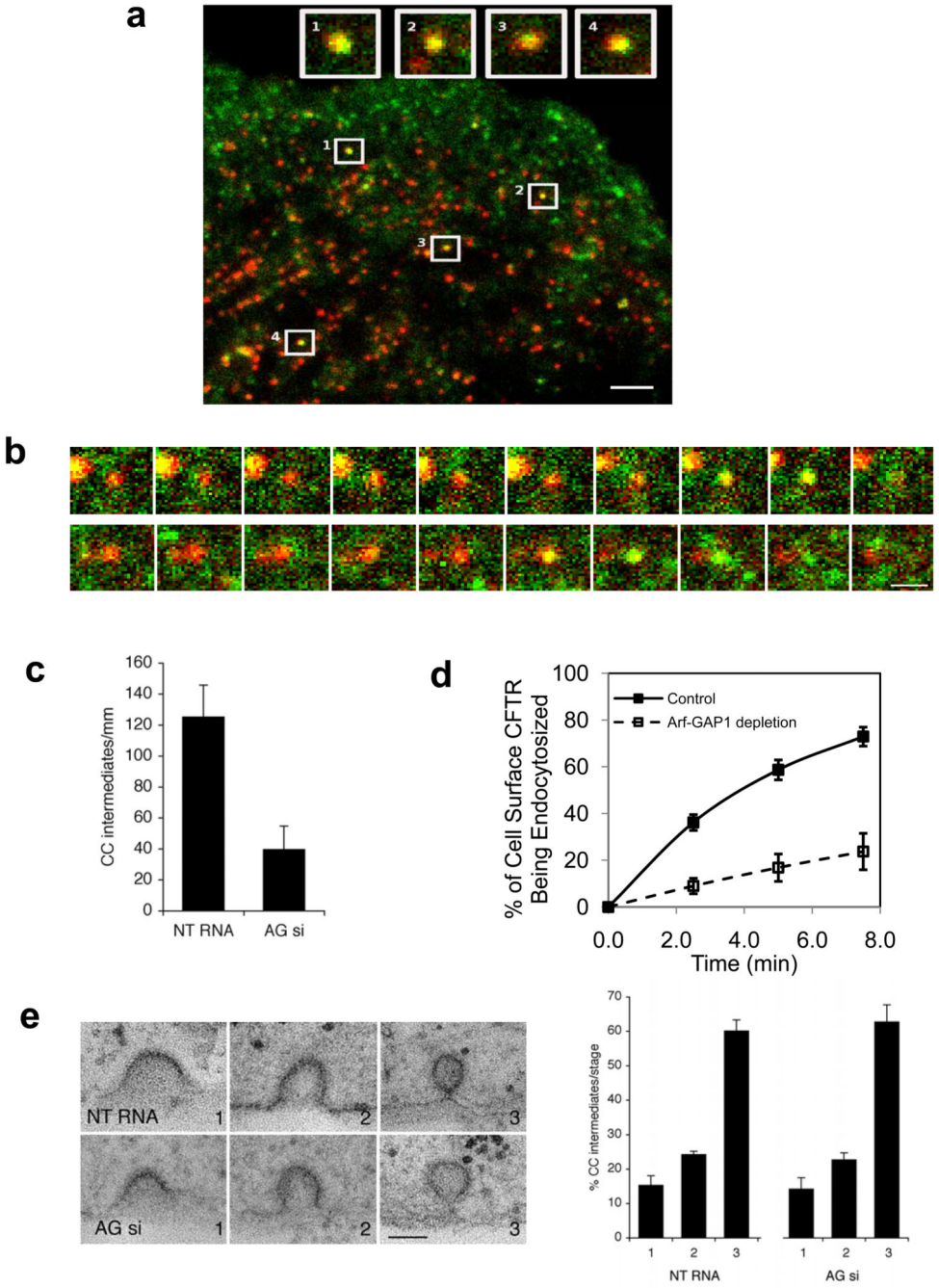

Figure 5. ARFGAP1 affects coated pits formation

a. Colocalization of ARFGAP1 with clathrin in coated pits. BSC-1 cells transfected with GFP-tagged ARFGAP1 and mCherry-tagged clathrin light chain (CLC) were examined by TIR-FM. The merged view shows colocalization of the two proteins; bar, 2 um. Insets highlight examples of coated pits found to have both ARFGAP1 (green) and clathrin (red). b. Dynamic association of ARFGAP1 with clathrin in coated pits. BSC-1 cells transfected with GFP-ARFGAP1 and mCherry-CLC and then examined by TIR-FM with live-imaging. Two examples are shown, with images captured every 3 seconds; bar, 1 μm.

c. Depletion of ARFGAP1 reduces the level of coated pits. HeLa cells were treated with siRNA conditions as indicated. All forms of clathrin coated (CC) intermediates were counted and then divided by the length of the plasma membrane. Seven cells were randomly selected from each condition to obtain the mean with standard deviation. Difference between two conditions is significant ($p<0.05$).

d. Depletion of ARFGAP1 inhibits the endocytosis of CFTR. CFBE41o- cells expressing WT-CFTR were polarized and then treated with siRNA conditions as indicated. The level of internalized CFTR was then quantified. The mean with standard error from three experiments is shown. Difference between two conditions (except time = 0) is significant ($p<0.05$).

e. Depletion of ARFGAP1 does not induce a particular stage of coated pit formation to accumulate. The different stages of coated pit formation, with representative images for each stage shown (left; bar, 100 nm), were detected by EM, and then quantified. The mean from three experiments with standard deviation is shown (right). Difference between corresponding stages is insignificant ($p>0.05$).

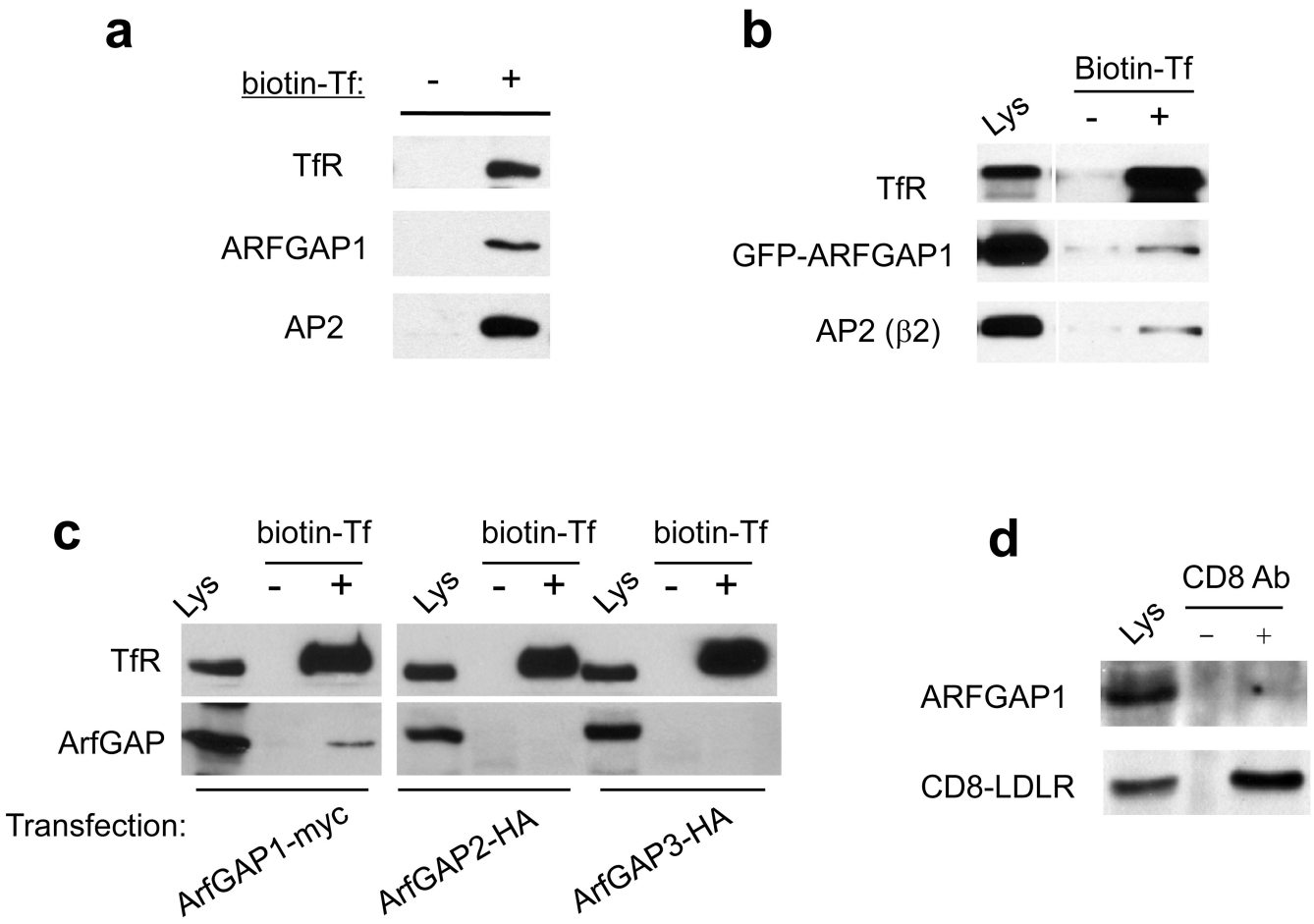

Figure 6. ARFGAP1 and AP-2 interact specifically with surface TfR

a. Endogenous surface TfR interacts with endogenous forms of ARFGAP1 and AP-2 in vivo. Biotin-labeled Tf was bound to the surface of HeLa cells followed by isolation using streptavidin beads, and then immunoblotting for proteins indicated.

b. GFP-tagged ARFGAP1 associates with endogenous forms of surface TfR and AP-2. BSC-1 cells were transfected with GFP-tagged ARFGAP1. Cells were then bound with biotin-labeled Tf, followed by incubation of cell lysate with streptavidin beads, and then immunoblotting for proteins indicated.

c. Surface TfR does not associate with ARFGAP-2 or ARFGAP3. HeLa cells were transfected with myc-tagged ARFGAP1, or HA-tagged forms of ARFGAP-2 or ARFGAP3. Cells were then bound with biotin-labeled Tf, and then lysed, followed by incubation of cell lysate with streptavidin beads, and then immunoblotting for proteins as indicated. ARFGAPs were detected through antibodies against the epitope tag.

d. A surface form of LDLR does not associate with ARFGAP1. HeLa cells that stably expressed CD8-LDLR were first incubated with anti-CD8 antibody. After this surface binding, cells were lysed and then incubated with protein A beads, followed by immunoblotting for proteins as indicated.

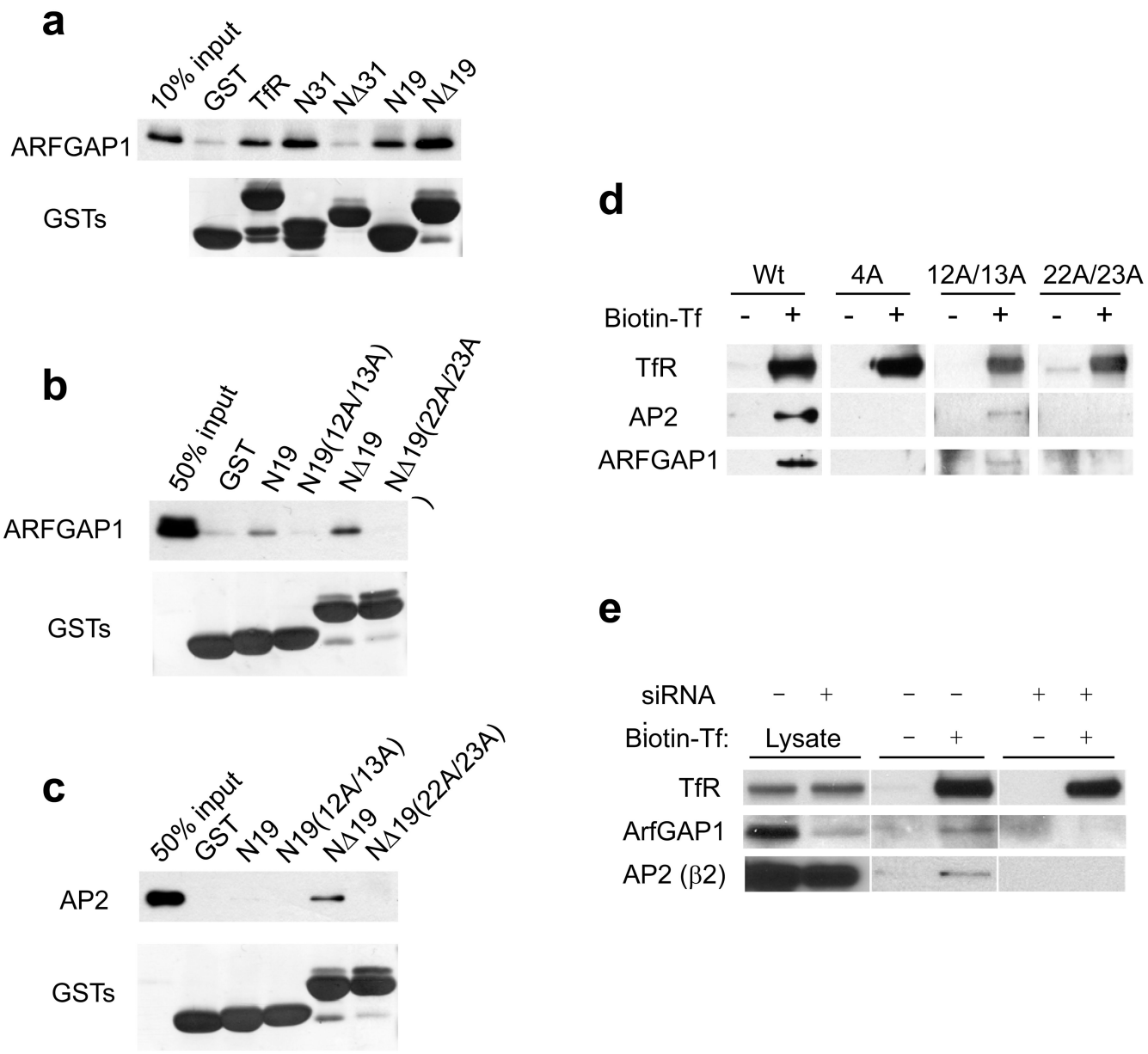

Figure 7. Characterizing the binding of TfR by ARFGAP1 and AP-2

a. Pulldown assays were performed using TfR constructs as indicated for incubation with recombinant ARFGAP1, followed by immunoblotting for ARFGAP1. GST fusion proteins were detected by Coomassie staining.

b. Pulldown assays were performed using TfR constructs as indicated for incubation with recombinant ARFGAP1, followed by immunoblotting for ARFGAP1. GST fusion proteins were detected by Coomassie staining. Point mutations within particular truncation constructs are indicated within parentheses.

c. Pulldown assays were performed using TfR constructs as indicated for incubation with purified AP-2, followed by immunoblotting for β2-adaptin. GST fusion proteins were

detected by Coomassie staining. Point mutations within particular truncation constructs are indicated within parentheses.

d. Effects on the association of surface TfR with ARFGAP1 and AP-2 upon mutating sorting signals in TfR. Biotin-labelled Tf was bound to the surface of mutant CHO (TRVb) cells that expressed different full-length TfR forms (either wild-type or different point mutations as indicated), followed by isolation using streptavidin beads, and then immunoblotting for proteins indicated. The “4A” construct contains alanine substitutions at residues 12, 13, 22, and 23 of TfR.

e. Association of surface TfR with AP-2 requires ARFGAP1. BSC-1 cells were treated with siRNA against ARFGAP1. Biotin-labeled Tf was bound to the surface of BSC-1 cells, followed by isolation using streptavidin beads, and then immunoblotting for endogenous proteins as indicated. Cell lysates were also directly immunoblotted for proteins in conditions as indicated.

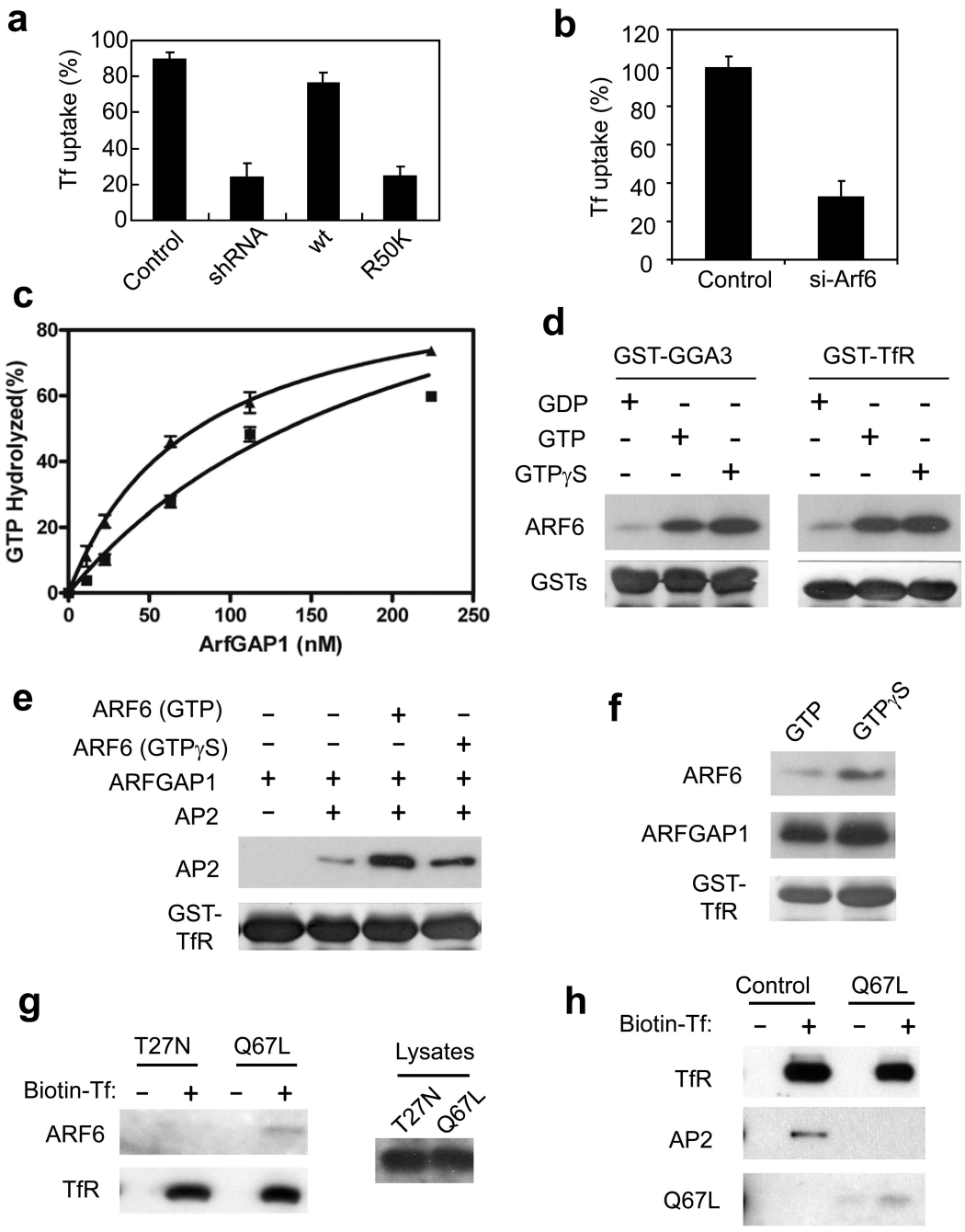

Figure 8. The GAP activity of ARFGAP1 is important for TfR endocytosis

a. The GAP activity of ARFGAP1 is important for TfR endocytosis. BSC-1 cells that stably expressed shRNA against ARFGAP1 were transfected with constructs as indicated. Uptake of biotin-Tf at 10 minutes was then quantified. The mean with standard error from three experiments is shown. Difference between the condition of shRNA and rescue by Wt is significant ($p<0.05$). Difference between the condition of shRNA and rescue by R50K is insignificant ($p>0.05$).

b. Depletion of ARF6 inhibits Tf uptake. BSC-1 cells were treated with siRNA against ARF6. Uptake of biotin-Tf at 10 minutes was then quantified. The mean with standard error from three experiments is shown. Difference between the two conditions is significant ($p<0.05$).

c. AP-2 enhances GAP activity of ARFGAP1 toward ARF6. The GAP assay was performed using ARF6 as the substrate, and either with (triangles) or without (squares) AP-2. The mean from three experiments with standard error is shown.

d. Binding of ARF6 to TfR is activation-dependent. ARF6 was confirmed functionally for its activation using the effector domain of GGA3 in a pulldown experiment (left panel). ARF6 forms were also incubated with GST-TfR in another pulldown experiment (right panel).

e. GAP activity of ARFGAP1 optimizes the binding of AP-2 to TfR. GST-TfR was incubated sequentially with ARF6 (containing different nucleotide bound, as indicated), followed by ARFGAP1, and then AP-2.

f. Deactivation of ARF6 by ARFGAP1 releases ARF6 from binding to TfR. ARF6 loaded with GTP forms as indicated were incubated with GST-TfR along with ARFGAP1 in a pulldown experiment.

g. Activation-dependent binding of ARF6 to surface TfR. BSC-1 cells were transfected with point mutant forms of ARF6 as indicated. Surface TfR was then isolated through biotin-Tf binding to cell surface, followed by incubation with streptavidin beads. Immunoblotting was then performed for proteins as indicated.

h. Constitutively activated form of ARF6 (Q67L) reduces the binding of AP-2 to surface TfR. BSC-1 cells were transfected with ARF6-Q67L or mock transfected. Surface TfR was then isolated as described above, followed by immunoblotting for associated proteins as indicated.